Asian Journal of Chemistry; Vol. 38, No. 5 (2026), 1234-1244

ASIAN JOURNAL OF CHEMISTRY

https://doi.org/10.14233/ajchem.2026.35581

Adsorptive Removal of Imidacloprid from Water Using Seed-Derived Lignocellulosic Bioadsorbents: Adsorption Mechanisms and Kinetic Insights

SAYYADA ZEBA BAKHTIYAR and RASHMI VERMA*

Department of Chemistry, Dr. C.V. Raman University, Bilaspur-495113, India

*Corresponding author: E-mail: rashmiverma@cvru.ac.in

Received: 8 January 2026 *Accepted*: 21 March 2026 *Published online*: 4 May 2026 AJC-22348

The present study investigates the removal of imidacloprid and related pesticide residues from contaminated water using seed-derived bioadsorbents. Bioadsorbents prepared from *Mangifera indica*, *Litchi chinensis* and *Ziziphus jujuba* seeds were characterised by scanning electron microscopy (SEM), X-ray diffraction (XRD) and Fourier transform infrared spectroscopy (FTIR) to examine surface morphology, structural features and functional groups responsible for adsorption. Instrumental analyses of contaminated water using high-performance liquid chromatography (HPLC) and gas chromatography-mass spectrometry (GC-MS) confirmed the presence of pesticide residues. Batch adsorption experiments evaluated the influence of bioadsorbent dose and contact time on removal efficiency. Kinetic analysis indicated that the adsorption process followed pseudo-second-order kinetics. Furthermore, adsorption behaviour was analysed using Langmuir, Freundlich and Temkin isotherm models. Post-adsorption GC-MS analysis showed a clear and significant reduction in pesticide-related signals, indicating effective removal of pesticide compounds after the adsorption process. Among the tested materials, *Ziziphus jujuba* exhibited the highest adsorption performance followed by *M. indica* and *L. chinensis*.

Keywords: Bioadsorption, Imidacloprid, Seed-derived bioadsorbents, Adsorption isotherms, Kinetic modelling.

INTRODUCTION

Water is essential for ecological balance, human health and socio-economic activities. Freshwater systems are increasingly threatened by chemical contamination from population growth, agriculture and industrialisation, with pesticides emerging as a major concern due to their widespread use and persistence in the environment [1-3]. Runoff from agricultural fields, improper disposal and leaching processes often transport pesticide residues into rivers, lakes and groundwater, leading to the deterioration of water quality and posing risks to aquatic organisms and human populations [4,5]. The presence of pesticide contaminants in water bodies has been associated with several ecological and health-related consequences. These compounds can disrupt aquatic food chains, affect microbial communities and accumulate in biological tissues through bioaccumulation and biomagnification processes [6-8]. Moreover, prolonged exposure to pesticide-contaminated water may lead to toxicological effects in humans including neurological, endocrine and developmental disorders [9]. Therefore, the removal of pesticide residues from water has become an important research focus in environmental remediation and sustainable water management.

Among the available water treatment technologies, adsorption has emerged as one of the most effective and environmentally compatible methods for contaminant removal. Adsorption processes are widely recognised for their operational simplicity, high removal efficiency and ability to treat low concentrations of pollutants without generating harmful secondary byproducts [10-12]. In recent years, increasing attention has been directed toward the development of bio-based adsorbents derived from agricultural or plant residues. These materials are renewable, cost-effective and environmentally sustainable, offering an attractive alternative to conventional synthetic adsorbents [13-15]. Plant-derived biomass materials are particularly promising because of their lignocellulosic composition, porous structure and surface functional groups that facilitate interactions with organic contaminants. In this context, seed residues from economically important plant species can serve as valuable precursors for the preparation of biochar-based adsorbents. *Mangifera indica* L. (mango), *Litchi chinensis* Sonn. (lychee) and *Ziziphus jujuba* Mill.

(jujube) are widely cultivated fruit-bearing species that generate substantial quantities of seed waste during processing. These seeds contain carbon-rich lignocellulosic components that can be converted into biochar materials with potential adsorption properties [16-18]. Therefore, the present study aims to prepare seed-derived biochar from *M. indica*, *L. chinensis* and *Z. jujuba* and evaluate their efficiency for pesticide removal from aqueous systems. The adsorption behaviour of the prepared bioadsorbents was assessed through batch experiments and adsorption isotherm modelling in order to better understand their removal performance and potential application in sustainable water purification strategies.

EXPERIMENTAL

Plant collection: Seeds of *Mangifera indica* L., *Litchi chinensis* Sonn. and *Ziziphus jujuba* Mill., were collected from the Surajpur region, Champaknagar, India (latitude 23.220º N and longitude 82.850º E). The collected seeds were thoroughly cleaned to remove dust and adhering debris, shade dried for 7-8 days under ambient laboratory conditions (~ 25-30 ºC) until constant weight was obtained and stored in airtight containers until further analysis. All three seed specimens were submitted for botanical authentication to the Botanical Survey of India (BSI), Allahabad, Uttar Pradesh, where a combined specimen representing all species was confirmed under the reference no. S.B.V.S./M.K.K./Tech./2025-26/327.

Preparation of bioadsorbent: The shade-dried and powdered seed materials were subjected to thermal and chemical activation to enhance their adsorption efficiency. Approximately 100 g of each seed powder was placed in a ceramic crucible and carbonised in a muffle furnace at 400-450 ºC for 2 h to promote partial pyrolysis and increase surface porosity. The thermally carbonised material was then chemically activated using 1 M H_3PO_4 at an impregnation ratio of 1:3 (w/v). The mixture was allowed to incubate for 24 h to ensure uniform penetration of the activating agent. After incubation, the samples were thoroughly washed with distilled water until a neutral pH was achieved to remove residual acid. The washed material was oven-dried at 105 ºC and subsequently sieved through a 250 μm mesh to obtain uniform activated bioadsorbent particles. The final activated bioadsorbents were stored in airtight, moisture-free containers until further use in adsorption experiments [19-21].

Characterisation: The surface morphology was examined by SEM after drying and gold sputter-coating, providing information on texture, porosity and particle aggregation relevant to adsorption performance. Crystallinity and phase composition were analysed by XRD using Cu*K*α radiation over a 2θ range of 5º-80º, enabling assessment of crystalline and amorphous structures. Functional groups involved in adsorption were identified by FTIR in the range of 4000-400 cm^{-1} using KBr pellet method, revealing surface-active groups such as hydroxyl, carboxyl and carbonyl functionalities.

Collection and analysis of pesticide-contaminated water samples: Pesticide contaminated water samples were collected from agricultural runoff channels located in the Surajpur-Champaknagar region, where routine farming activities contribute to chemical accumulation in surface waters. Sampling was performed during active irrigation periods to ensure the representative contamination levels. Water samples were collected in pre-cleaned 1 L Amber glass bottles, rinsed three times with the sampling water before final collection to avoid cross-contamination. All samples were maintained at 4 ºC in the insulated ice boxes and transported to the laboratory within 4-6 h of sampling. Upon arrival, the samples were filtered through 0.45 μm membrane filters to remove suspended particulates and stored at 4 ºC until further analysis. No preservatives were added to avoid interference with subsequent adsorption experiments or HPLC quantification. All sampling, handling and storage procedures followed standard guidelines to ensure the integrity and stability of pesticide residues for analytical evaluation.

Chemical composition and pesticide residue screening (GC-MS): Gas chromatography-mass spectrometry (GC-MS) was used to confirm the presence and degradation of pesticide residues before and after adsorption. Samples were extracted using standard liquid-liquid extraction protocols and filtered through a 0.22 μm PTFE membrane. The GC-MS system was operated in electron impact (EI) mode with a capillary column suited for organophosphate/organochlorine pesticide analysis. Chromatographic conditions (temperature program, carrier gas flow rate) were optimised to the ensure selective separation and quantification. Mass spectra were matched with NIST library entries for the compound identification.

Batch adsorption experiments: Adsorption studies were carried out under controlled conditions to determine removal efficiency [22-24]. Briefly, 100 mL pesticide solution was placed in Erlenmeyer flasks and 0.5-2.0 g of bioadsorbent was added. The mixtures were agitated on a rotary shaker at 150 rpm for 60-180 min. Parameters such as pH (3-9), contact time, adsorbent dosage and initial pesticide concentration were optimised. After equilibrium, samples were filtered using 0.22 μm membrane filters. Removal efficiency (%) was calculated using the following eqn. 1:

$$\text{Removal (\%)} = \frac{C_o - C_e}{C_o} \times 100 \quad (1)$$

where C_o = initial concentration and C_e = equilibrium concentration.

HPLC quantification of residual pesticides: Residual pesticide concentrations in untreated water were quantified using high-performance liquid chromatography (HPLC). A C_{18} reverse-phase column (250 × 4.6 mm, 5 μm) was used with a mobile phase of acetonitrile-water (70:30, v/v) at a flow rate of 1 mL/min. UV detection wavelengths were selected according to the absorption maxima of the target pesticides. The injection volume was 20 μL and each sample was analysed in triplicate. Calibration curves were prepared using certified pesticide standards and quantification was performed by peak-area comparison.

Kinetic and isotherm modelling: To understand the adsorption mechanism, kinetic models, pseudo-first order and pseudo-second order were applied. Model parameters were derived using nonlinear regression analysis [25-28].

Pseudo-first-order kinetic model: This model assumes that the adsorption rate is proportional to the number of unoccupied active sites and is represented as follows:

$$\ln(q_e - q_t) = \ln q_e - k_1 t \quad (2)$$

where q_t = amount of pesticide adsorbed at time t (mg/g), q_e = amount of pesticide adsorbed at equilibrium (mg/g), k_1 = pseudo-first-order rate constant (min^{-1}), t = contact time (min).

Pseudo-second-order kinetic model: Assumes chemisorption involving electron sharing or exchange between sorbent and adsorbate and is represented as follows:

$$\frac{1}{q_t} = \frac{1}{K_2 q_e^2} + \frac{t}{q_e} \quad (3)$$

where q_t = adsorption capacity at time t (mg/g), q_e = adsorption capacity at equilibrium (mg/g), k_2 = pseudo-second-order rate constant (g mg^{-1} min^{-1}), t = adsorption time (min).

Adsorption isotherm analysis: Adsorption isotherm models are widely used to describe the interaction between adsorbate molecules and adsorbent surfaces and to evaluate the adsorption capacity of the material. In this study, equilibrium adsorption data obtained under optimised conditions were analysed using Langmuir, Freundlich and Temkin isotherm models to better understand the adsorption mechanism of pesticide molecules onto the seed-derived bioadsorbents [29-31].

Langmuir isotherm: The Langmuir isotherm assumes monolayer adsorption on a homogeneous surface with a finite number of identical active sites. The model can be expressed as follows:

$$q_e = \frac{q_{max} K_L C_e}{1 + K_L C_e} \quad (4)$$

where q_e represents the equilibrium adsorption capacity (mg g^{-1}); q_{max} is the maximum monolayer adsorption capacity (mg g^{-1}); K_L is the Langmuir adsorption constant (L mg^{-1}) and C_e is the equilibrium concentration of pesticide in solution (mg L^{-1}).

Freundlich isotherm: The Freundlich isotherm describes adsorption on heterogeneous surfaces and assumes multilayer adsorption. The model is expressed as follows:

$$q_e = K_F C_e^{1/n} \quad (5)$$

where K_F is the Freundlich adsorption constant related to adsorption capacity and n represents the adsorption intensity.

Temkin isotherm: Temkin isotherm considers the adsorbate–adsorbent interactions and assumes that the heat of adsorption decreases linearly with increasing surface coverage. The Temkin model is represented as follows:

$$q_e = B \ln(K_T C_e) \quad (6)$$

where K_T is the Temkin equilibrium binding constant and B is related to the heat of adsorption.

RESULTS AND DISCUSSION

Morphological studies: The SEM micrographs of *Z. jujuba*, derived material (Fig. 1), recorded at magnifications from 5 to 50 μm, reveal a hierarchical and irregular surface morphology. Granular protrusions, fragmented fibers and shallow fissures indicate disruption of the lignocellulosic matrix during processing. Interconnected channels and elongated cavities form a porous network, while wider cracks at higher magnification confirm macroporosity. Such rough, multi-scale structural features increase surface accessibility and provide abundant active sites, thereby enhancing adsorption efficiency toward pesticide molecules.

The SEM micrographs of *L. chinensis*, derived biomaterial (Fig. 2), obtained at magnifications from 5 to 50 μm, reveal a heterogeneous and hierarchically structured surface. Fine granularity, fibrillar fragments and shallow fissures indicate disruption of the lignocellulosic matrix during processing. Interconnected channels and irregular voids form a porous framework, while wider fissures at higher magnification confirm macroporous domains. These structural irregularities increase surface roughness and accessibility, providing potential active sites for interaction and adsorption of pesticide molecules.

The SEM micrographs of *M. indica*, derived biomaterial (Fig. 3), also reveal a heterogeneous lignocellulosic structure with distinct porous features. Granular deposits, fibrillar domains and shallow cracks indicate disruption of the biomass matrix during processing. Interconnected channels and elongated cavities suggest the development of an internal pore network, while wider fissures at higher magnification confirm macroporosity. These multi-scale structural characteristics enhance surface accessibility and facilitate adsorption of pesticide molecules.

XRD studies: X-ray diffraction (XRD) analysis was performed to examine the structural characteristics of the *Z. jujuba* seed, derived bioadsorbent (Fig. 4a). The diffraction pattern exhibits a broad peak within 2θ ≈ 20-30º, indicating a predominantly amorphous carbon structure originating from lignocellulosic biomass components. The absence of sharp crystalline reflections confirms structural disorder produced during the carbonisation and activation processes. Minor low intensity peaks at higher 2θ values may correspond to trace inorganic mineral residues present in the seed matrix.

The diffractogram of bioadsorbent *L. chinensis* seed, also exhibits a broad diffraction peak centered at 2θ ≈ 18-25º, indicating the formation of a predominantly amorphous carbon structure originating from lignocellulosic biomass. This broad band reflects the disordered arrangement of carbon atoms generated during carbonisation and activation, accompanied by the disruption of native crystalline cellulose domains. Minor intensity variations at higher diffraction angles may correspond to residual mineral constituents inherent to the seed matrix. Similarly, the diffractogram of *M. indica* seed, (Fig. 4c) displays a broad and diffused peak within 2θ ≈ 20-30º, indicating the formation of a predominantly amorphous carbon structure after thermal and chemical activation of the lignocellulosic biomass. The absence of sharp crystalline reflections suggests significant disruption of the native cellulose framework and transformation into a disordered carbon matrix. Minor low-intensity features at higher diffraction angles may correspond to residual inorganic constituents present in the seed material. Thus, based on these results, in all cases, an amorphous and heterogeneous structure enhances surface irregularity and increases the availability of active adsorption sites, thereby improving interaction with pesticide molecules during adsorption.

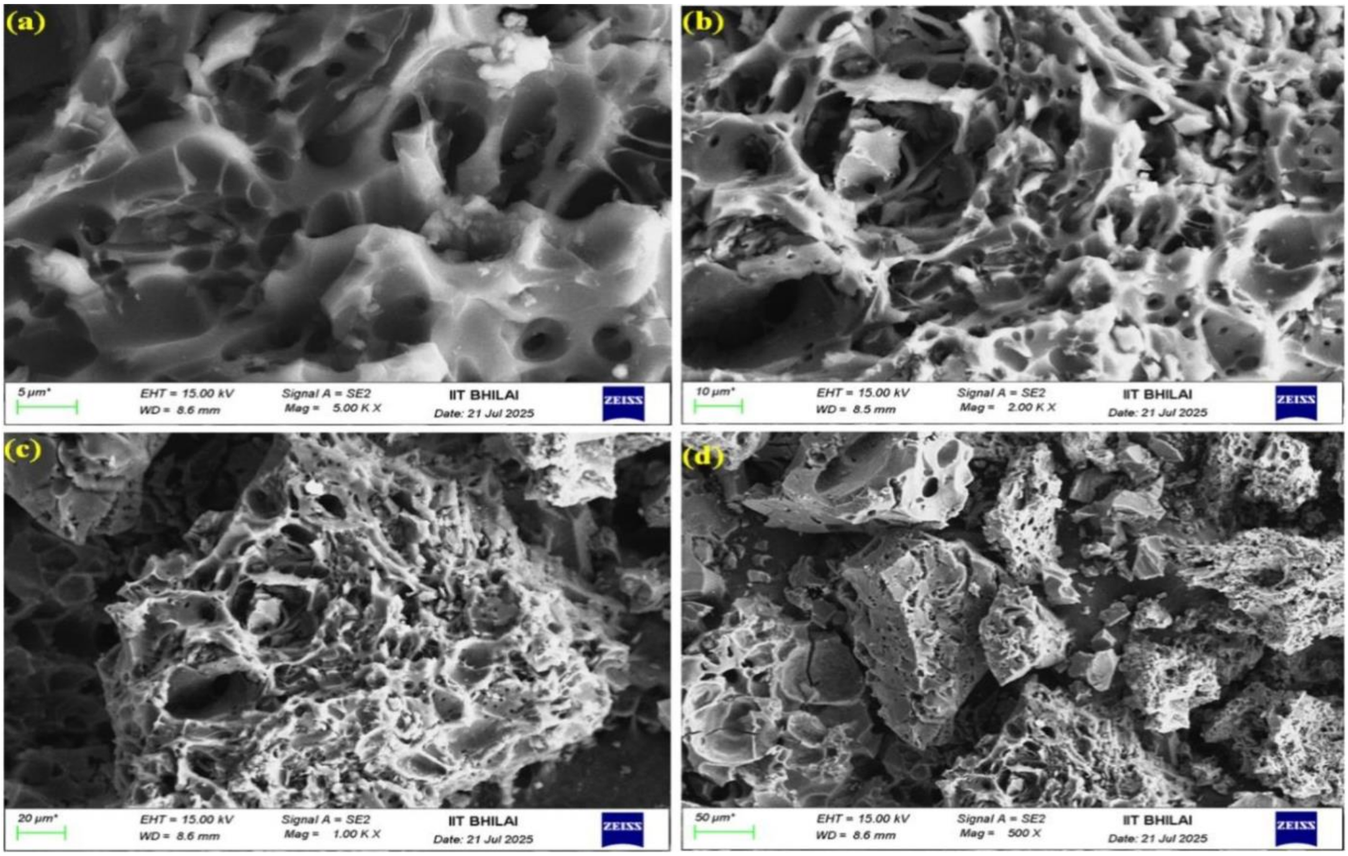

Fig. 1. SEM micrographs of *Ziziphus jujuba* biomaterial at different magnifications, (a) 5 µm, (b) 10 µm, (c) 20 µm and (d) 50 µm

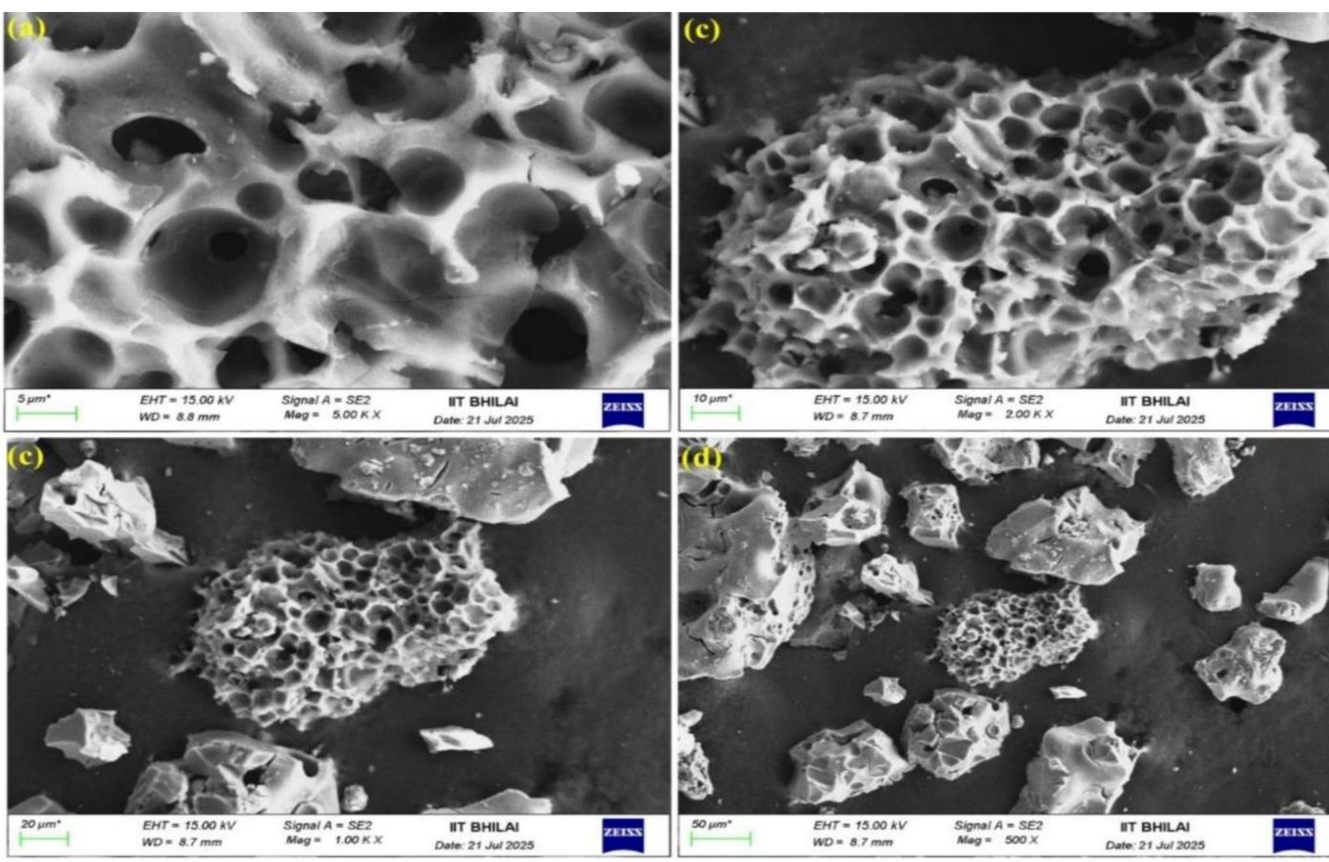

Fig. 2. SEM micrographs of *Litchi chinensis* biomaterial at different magnifications, (a) 5 µm, (b) 10 µm, (c) 20 µm and (d) 50 µm

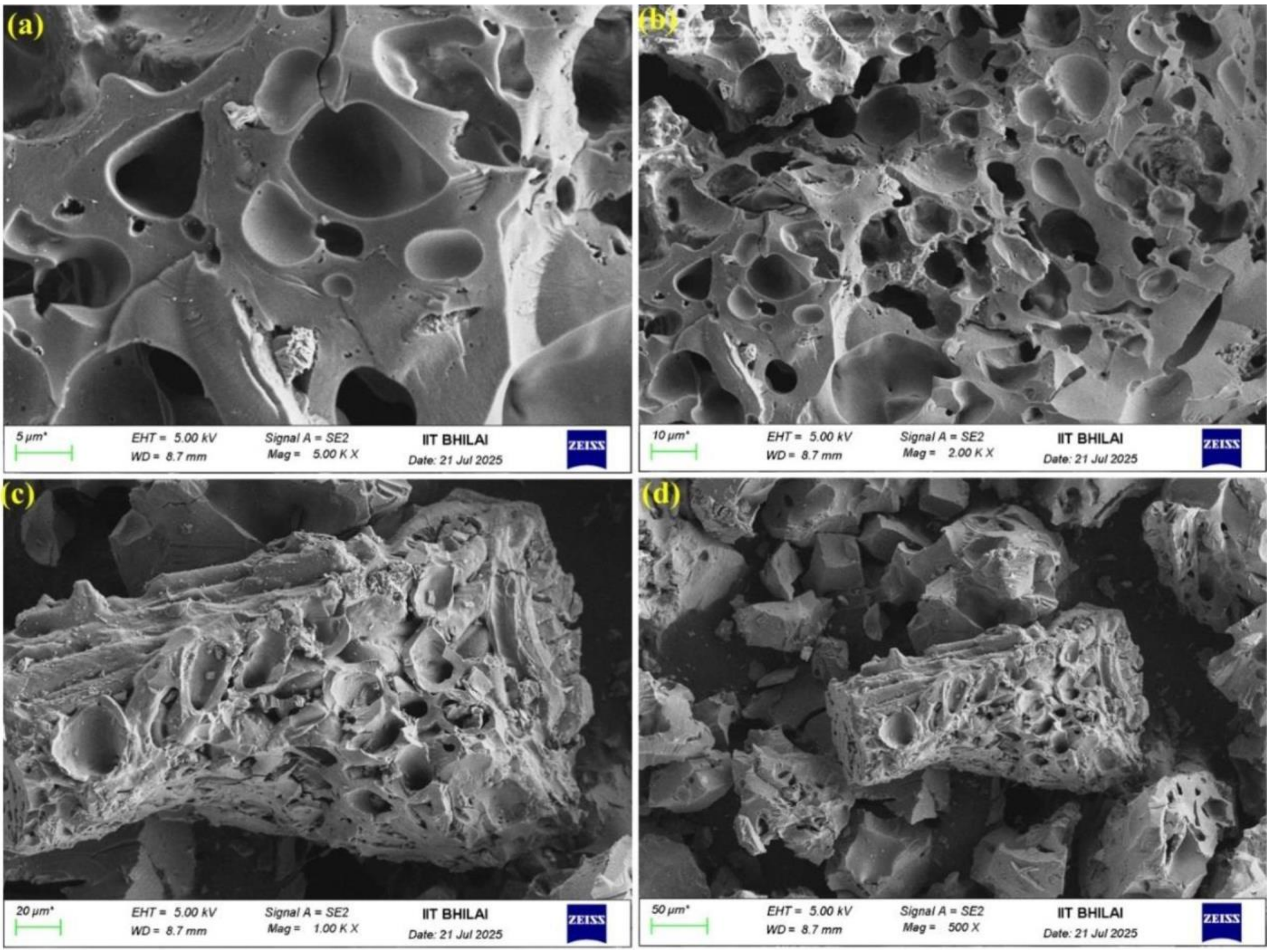

Fig. 3. SEM micrographs of *Mangifera indica* biomaterial at different magnifications, (a) 5 µm, (b) 10 µm, (c) 20 µm and (d) 50 µm

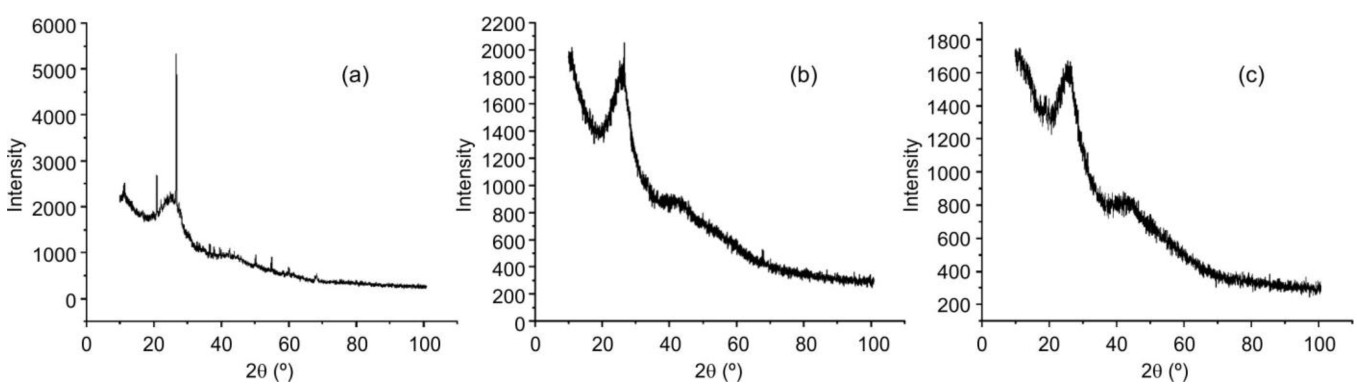

Fig. 4. XRD pattern of (a) *Ziziphus jujuba*, (b) *Litchi chinensis* and (c) *Mangifera indica* seed derived bioadsorbent

FTIR studies: The FTIR spectra of all the studied *Z. jujuba*, *L. chinensis* and *M. indica* seed-derived bioadsorbents consistently reveal the presence of key surface functional groups responsible for the adsorption behavior (Fig. 5). The broad bands observed at ~3421-3416 cm^{-1} correspond to –OH stretching vibrations of hydroxyl groups from cellulose and hemicellulose, indicating their role in hydrogen bonding with pesticide molecules. Peaks in the range of 2922–2926 and 2854-2851 cm^{-1} are attributed to aliphatic C–H stretching of the lignocellulosic framework. The bands around 1735-1732 cm^{-1} confirm the presence of carbonyl (C=O) groups such as esters and carboxylic functionalities, while signals at ~1638-1632 cm^{-1} are associated with aromatic C=C structures originating from lignin. The C–O and C–O–C vibrations across all samples indicate oxygenated functional groups that enhance the electrostatic interactions and surface reactivity. The similarity in functional group distribution across these bioadsorbents highlights their lignocellulosic nature and supports their effectiveness in facilitating hydrogen bonding and electrostatic interactions during pesticide adsorption [32].

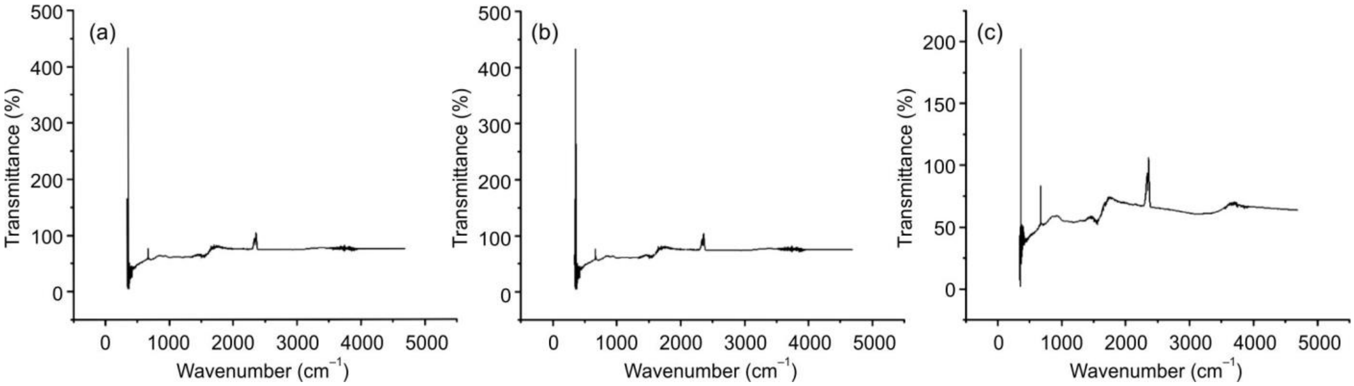

Fig. 5. FTIR spectrum of (a) *Ziziphus jujuba*, (b) *Litchi chinensis* and (c) *Mangifera indica* seed-derived bioadsorbent

GC-MS analysis of untreated water sample: GC-MS analysis of the pesticide contaminated water sample revealed a complex chromatographic profile, confirming the presence of multiple organic contaminants. The total ion chromatogram (TIC) (Fig. 6) exhibited several well-resolved peaks distributed across the retention time range of approximately 2-20 min, indicating the coexistence of compounds with varying volatility and polarity. Compound identification was carried out by comparing the acquired mass spectra with the NIST mass spectral library (Table-1). GC-MS spectrum showed the characteristic fragmentation patterns, enabling identification of nitrogen-containing heterocycles, fluorinated compounds, esters and aromatics. Diagnostic ions for nitro, cyano, amide and fluorinated groups supported these assignments, while repeated detection of related compounds at different retention times suggests the presence of pesticide residues and ongoing transformation processes in the aquatic system.

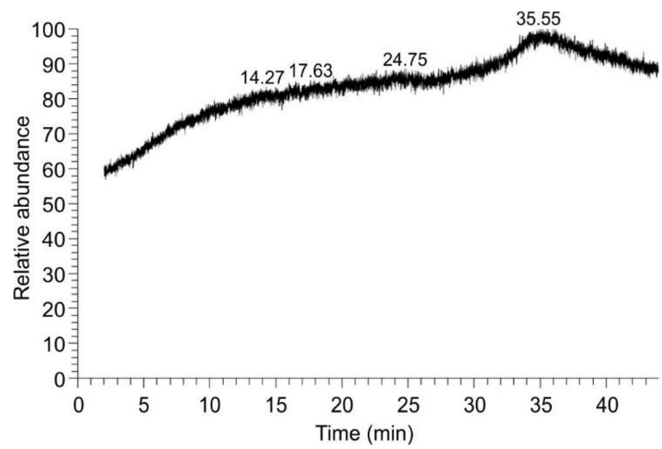

Fig. 6. Total ion chromatogram (TIC) of pesticide contaminated water sample analysed by GC-MS

HPLC analysis of imidacloprid in water sample: The HPLC analysis of the water sample for imidacloprid revealed a clear, well-resolved chromatographic peak at a retention time of 6.21 min, matching the standard imidacloprid peak (Fig. 7). The water sample showed a detector response of 3,218 mAU, corresponding to an imidacloprid concentration of 1.36 mg L^{-1} based on the calibration curve (0.10-5.00 mg L^{-1}). The peak was symmetric with no interference, indicating good resolution and selective detection, confirming the presence of imidacloprid at measurable levels in the sample.

Batch adsorption studies: Batch adsorption experiments were performed to evaluate the pesticide removal efficiency of seed-derived bioadsorbents prepared from *M. indica*, *L. chinensis* and *Z. jujuba* under controlled laboratory conditions. The experiments were carried out at a fixed initial pesticide concentration of 10 mg L^{-1} and a constant temperature of 25 ºC, while the bioadsorbent dose (0.5-2 g L^{-1}) and contact time (30-90 min) were systematically varied to investigate their influence on adsorption performance (Table-2). An increase in bioadsorbent dosage and contact time resulted in the enhancement of pesticide removal efficiency for all bioadsorbents. For *M. indica* seed biochar, the removal efficiency increased from 48.62 ± 1.02% at 0.5 g L^{-1} and 30 min to 81.27 ± 0.86% at 2 g L^{-1} and 90 min. A similar trend was observed for *L. chinensis* seed biochar, where the removal efficiency improved from 44.58 ± 1.08% to 78.15 ± 0.91% with increasing adsor-

TABLE-1
GC-MS IDENTIFIED ORGANIC CONTAMINANTS IN PESTICIDE CONTAMINATED WATER SAMPLE

RT (min)	Identified compound	m.f.	m.w. (g/mol)	Peak area (%)	Match probability (%)
2.47	8,9,9,10,10,11-Hexafluoro-4,4-dimethyl-3,5-dioxatetracyclo dodecane	$C_{12}H_{12}F_6O_2$	302	0.86	32.98
4.46	Pterin-6-carboxylic acid	$C_7H_5N_5O_3$	207	0.83	52.81
5.28	3-(Prop-2-enoyloxy) tetradecane	$C_{17}H_{32}O_2$	268	0.77	39.74
9.42	Hydrazine derivative (trace organic nitrogen compound)	H_4N_2	32	0.95	40.99
10.09	Trimethyl-hydroxymethyl cyclohexene derivative	$C_{15}H_{26}O$	222	0.81	22.04
12.74	Perfluoro (dibutylmethyl) amine	$C_9F_{21}N$	521	0.74	26.83
13.83	Pyrimidine, 4,6-dimethoxy-5-nitro-	$C_6H_7N_3O_4$	185	1.45	16.7
16.69	Perfluoro (dibutylmethyl) amine	$C_9F_{21}N$	521	0.76	53.84
20.33	Pyrazolo[1,5-*a*]pyridine, 3-methyl-2-phenyl-	$C_{14}H_{12}N_2$	208	1.16	90.69

TABLE-2
BATCH ADSORPTION EXPERIMENTAL CONDITIONS AND REMOVAL EFFICIENCY

Bioadsorbent type	Dose (g/L)	Initial pesticide concentration (mg/L)	Contact time (min)	pH	Temperature (ºC)	Removal efficiency (%)
M. indica seed Biochar	0.5	10	30	6.5	25	48.62 ± 1.02
	1.0	10	60	6.5	25	63.41 ± 0.94
	2.0	10	90	6.5	25	81.27 ± 0.86
L. chinensis seed Biochar	0.5	10	30	7.0	25	44.58 ± 1.08
	1.0	10	60	7.0	25	59.73 ± 0.97
	2.0	10	90	7.0	25	78.15 ± 0.91
Z. jujuba seed Biochar	0.5	10	30	6.8	25	51.24 ± 0.89
	1.0	10	60	6.8	25	67.93 ± 0.82
	2.0	10	90	6.8	25	84.66 ± 0.74

Values are expressed as mean ± SD (n = 3)

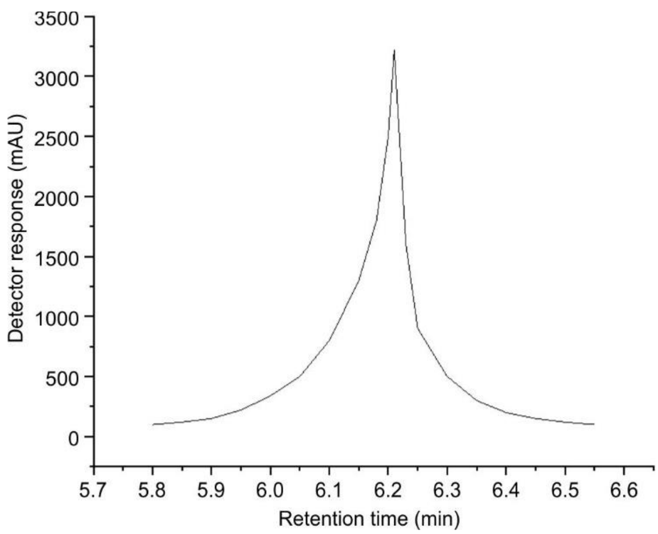

Fig. 7. HPLC chromatogram of imidacloprid in water sample

bent dose and contact time. Among the tested materials, *Z. jujuba* seed biochar exhibited the highest adsorption efficiency, reaching 84.66 ± 0.74% under the optimised experimental conditions (Fig. 8). The improved adsorption performance at higher adsorbent doses can be attributed to the availability of a greater number of active surface sites, while longer contact time facilitates enhanced interaction between pesticide molecules and the bioadsorbent surface.

Kinetic model validation and adsorption mechanism: To elucidate the adsorption mechanism and rate-controlling steps involved in pesticide removal, the experimental kinetic data were analysed using pseudo-first order (PFO) and pseudo-second order (PSO) kinetic models. A comparative evaluation of the experimental and model-predicted parameters provides valuable insight into the adsorption behaviour of the studied bioadsorbents (Table-3).

Fig. 9a presents a comparison between the experimental equilibrium adsorption capacity (q_e) and the values calculated

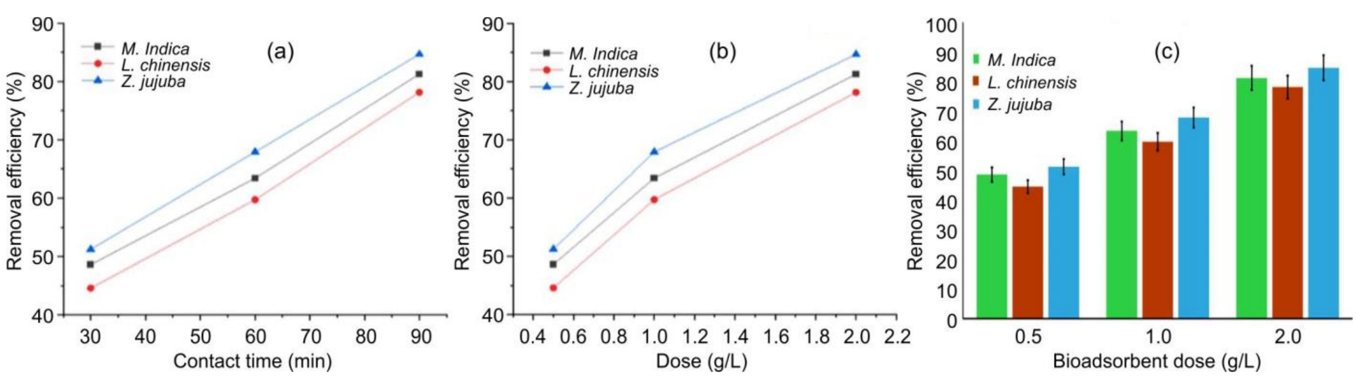

Fig. 8. (a) Effect of bioadsorbent dose on removal efficiency, (b) effect of contact time on removal efficiency, (c) removal efficiency of bioadsorbent doses (values are expressed as mean ± SD (n = 3)

TABLE-3
KINETIC PARAMETERS FOR PESTICIDE ADSORPTION INTO BIOADSORBENTS

Bioadsorbent	q_e (exp) (mg/g)	k_1 (min^{-1})	q_e (cal) (mg/g)	R^2	k_2 (g mg^{-1} min^{-1})	q_e (cal) (mg/g)	R^2
M. indica seed biochar	8.42	0.027	7.91	0.942	0.0056	8.40	0.996
L. chinensis seed biochar	7.65	0.024	7.18	0.937	0.0049	7.63	0.994
Z. jujuba seed biochar	9.12	0.031	8.70	0.951	0.0062	9.10	0.998

where, q_e (exp) = experimental adsorption capacity at equilibrium (mg/g), q_e(cal) = model-calculated adsorption capacity at equilibrium (mg/g), k_1 = pseudo-first-order rate constant (min^{-1}), k_2 = pseudo-second-order rate constant (g mg^{-1} min^{-1}), R^2 = coefficient of determination indicating goodness of fit.

using the pseudo-first-order kinetic model for all investigated bioadsorbents. The calculated q_e values obtained from the PFO model showed the reasonable proximity to the experimental data; however, slight differences suggest that the adsorption process cannot be fully represented by a model based primarily on physical adsorption phenomena. Fig. 9b illustrates the comparison between experimental q_e values and those predicted by the pseudo-second-order kinetic model. The calculated q_e values from the PSO model exhibited excellent agreement with the experimental results for all bioadsorbents, indicating that the adsorption kinetics are more accurately described by this model. This behaviour suggests the involvement of the chemisorption mechanisms, including electron sharing or exchange between pesticide molecules and functional groups present on the bioadsorbent surfaces. Fig. 9c depicts the model fitness comparison using the coefficient of determination (R^2). The consistently higher R^2 values obtained for the PSO model (> 0.99) further confirm its superior applicability in describing the adsorption kinetics. Fig. 9d compares the kinetic rate constants, where *Z. jujuba* seed biochar shows higher pseudo-second-order rate constants (k_2), correlating well with its enhanced adsorption performance. Thus, in all cases, the kinetic analysis demonstrates that pesticide adsorption onto seed-derived bioadsorbents predominantly follows pseudo-second-order kinetics.

Adsorption isotherms: The adsorption equilibrium data were analysed using Langmuir, Freundlich and Temkin isotherm models to better understand the adsorption behaviour of pesticide molecules onto the seed-derived bioadsorbents. The Langmuir model showed high correlation coefficients (R^2 = 0.984-0.991), indicating that adsorption predominantly occurs as a monolayer on relatively homogeneous active sites (Table-4). Among the materials studied, *Z. jujuba* exhibited the highest Langmuir adsorption capacity (q_{max} = 10.26 mg g^{-1}), aligning with its superior removal efficiency observed in batch experiments. The Freundlich model also demonstrated strong agreement (R^2 = 0.979-0.986), suggesting the presence of heterogeneous surface sites and possible multilayer

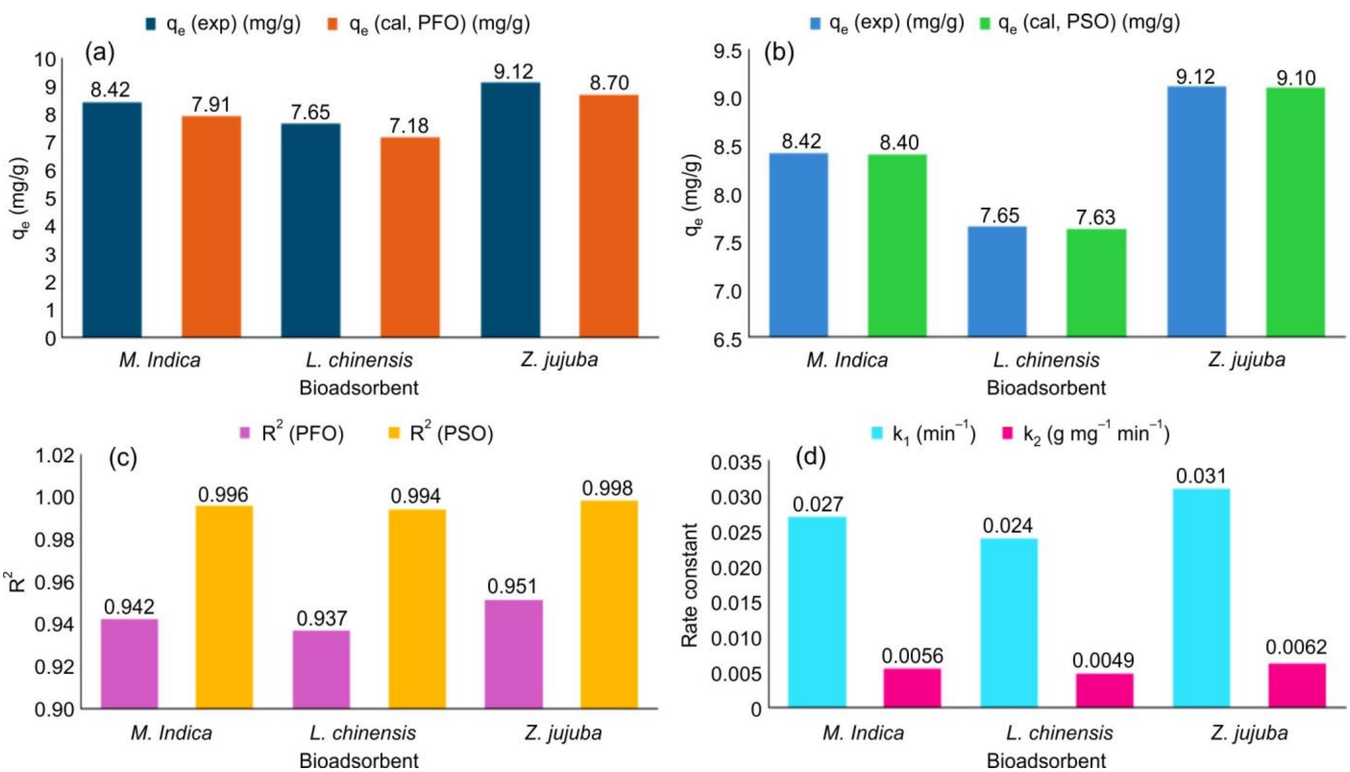

Fig. 9. (a) Experimental *vs*. calculated q_e (pseudo-first order), (b) experimental *vs*. calculated q_e (pseudo-second order) (c) model fitness comparison using R^2 (R^2 = coefficient of determination), (d) rate constant comparison (k_1 = pseudo-first-order rate constant (min^{-1}), k_2 = pseudo-second-order rate constant (g mg^{-1} min^{-1})

TABLE-4
ADSORPTION ISOTHERM PARAMETERS FOR PESTICIDE ADSORPTION ONTO SEED-DERIVED BIOADSORBENTS

Bioadsorbent	q_{max} (mg g^{-1})	K_L (L mg^{-1})	R^2 (Langmuir)	K_F [(mg g^{-1}) (L mg^{-1})$^{1/n}$]	n	R^2 (Freundlich)	K_T (L mg^{-1})	B (J mol^{-1})	R^2 (Temkin)
M. indica seed biochar	9.38	0.214	0.987	3.42	2.17	0.982	0.168	3.91	0.973
L. chinensis seed biochar	8.54	0.186	0.984	2.96	2.05	0.979	0.149	3.64	0.968
Z. jujuba seed biochar	10.26	0.243	0.991	3.88	2.31	0.986	0.192	4.18	0.978

where, q_{max} (mg g^{-1}) = Maximum monolayer adsorption capacity of the bioadsorbent, K_L (L mg^{-1}) = Langmuir adsorption constant related to adsorption affinity, K_F [(mg g^{-1})(L mg^{-1})$^{1/n}$] = Freundlich adsorption constant representing adsorption capacity, n = Freundlich adsorption intensity parameter indicating adsorption favourability, K_T (L mg^{-1}) = Temkin equilibrium binding constant, B (J mol^{-1}) = Temkin constant related to the heat of adsorption, R^2 = Correlation coefficient representing the goodness of fit of the isotherm model.

adsorption, with adsorption intensity values (n = 2.05-2.31) confirming favourable uptake. The Temkin model provided moderate correlation (R^2 = 0.968-0.978), indicating significant adsorbate–adsorbent interactions and a gradual decrease in heat of adsorption with increasing surface coverage. Higher Temkin constants for *Z. jujuba* seeds further support its stronger interaction with pesticide molecules (Table-4). Thus, all the studied models indicate that adsorption proceeds through a combination of monolayer and heterogeneous mechanisms, with *Z. jujuba* seeds as adsorbent demonstrating the most effective adsorption performance.

Comparative studies: A comparative overview of the reported biomass-derived adsorbents for the imidacloprid removal is shown in Table-5. Earlier studies have largely focused on chemically modified or single-source biochars to enhance adsorption capacity. In contrast, the present work investigates unmodified fruit seed-derived biochars from *M. indica*, *L. chinensis* and *Z. jujuba* as sustainable agro-waste resources for the removal of imidacloprid.

GC-MS analysis of the treated water sample: GC-MS analysis was further conducted to assess the pesticide removal efficiency of *M. indica*, *L. chinensis* and *Z. jujuba* seed-derived bioadsorbents. The untreated water sample showed multiple pesticide-related compounds with peak areas in the range of 0.74-1.45% (Table-1), confirming the presence of the organic contaminants. After adsorption treatment, all bioadsorbents produced a significant reduction in both the number and intensity of chromatographic peaks, indicating effective contaminant removal (Fig. 10). The *M. indica* bioadsorbent exhibited significant attenuation (≈80-90%), with only a few low-intensity peaks remaining at retention times around 2.01, 8.21, 16.06 and 22.15 min (Fig. 10a). The *L. chinensis* bioadsorbent showed a reduction of approximately 75-90%, with weak residual peaks at 2.01, 6.18, 8.81, 15.59 and 20.62 min, corresponding to trace organic fragments (Fig. 10b). The most pronounced removal was observed with *Z. jujuba*, which demonstrated the highest suppression of chromatographic signals (≈85-95%), leaving only minor peaks at 5.30, 14.93 and 21.48 min (Fig. 10c). The significant decrease in peak intensity across all treated samples confirms strong interactions between pesticide molecules and the functional groups present on the lignocellulosic surfaces of the bioadsorbents. Among the studied materials, *Z. jujuba* exhibited the most efficient adsorption performance, indicating its superior capability for the removal of imidacloprid and related pesticide residues from the aqueous systems.

Conclusion

This study systematically evaluated the potential of *M. indica*, *L. chinensis* and *Z. jujuba* seeds-derived bioadsorbents for the removal of imidacloprid and related pesticide residues from the contaminated water through comprehensive physicochemical characterisation, adsorption experiments, kinetic modelling, isotherm analysis and instrumental validation. The prepared bioadsorbents were successfully characterised using SEM, XRD and FTIR techniques. SEM analysis revea-

TABLE-5
COMPARISON OF ADSORPTION PERFORMANCE OF DIFFERENT BIOMASS-DERIVED ADSORBENTS REPORTED FOR IMIDACLOPRID REMOVAL FROM AQUEOUS SYSTEMS

Adsorbent	Source material	Maximum adsorption capacity (mg g^{-1})/Removal efficiency	Key observation	Ref.
Fe/Zn modified biochar	White melon seed shell	87.69% removal within 30 min	Enhanced adsorption due to metal oxide modification	[33]
Magnetic loofah sponge biochar	Loofah biomass	738 mg g^{-1}	Highly porous structure with excellent regeneration ability	[34]
Fe-Mg modified biochar	Water hyacinth biomass	114 mg g^{-1}	Improved adsorption due to surface complexation	[35]
Iron-modified activated biochar	Sugarcane bagasse	10.33 mg g^{-1}	Removal efficiency ~92% with Freundlich isotherm behaviour	[36]
Magnetic corn cob biochar	Corn cob agricultural waste	410 mg g^{-1}	High adsorption capacity with good regeneration potential	[37]

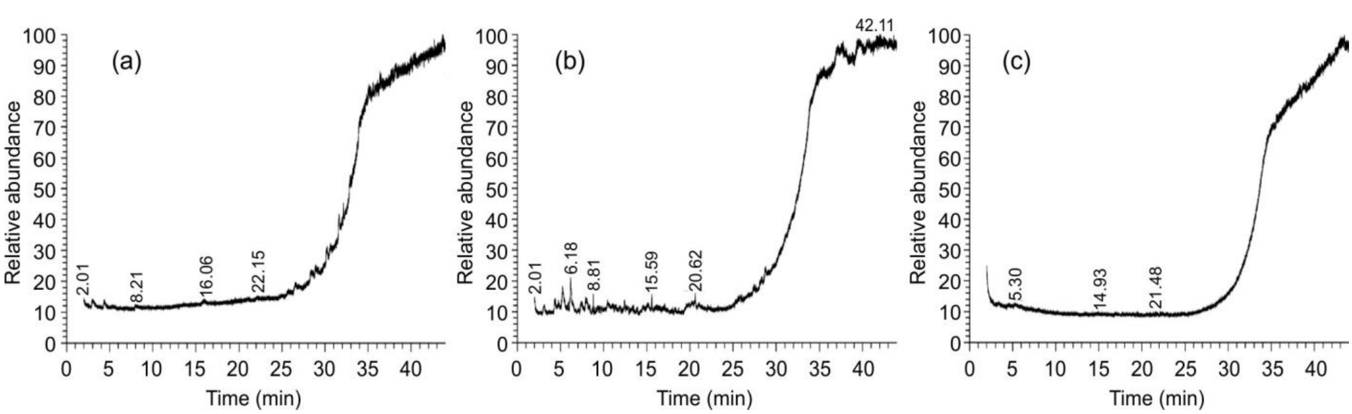

Fig. 10. GC-MS chromatograms of pesticide-contaminated water sample after adsorption using (a) *M. indica*, (b) *L. chinensis* and (c) *Z. jujuba* seed bioadsorbents

led heterogeneous, porous surfaces favourable for adsorption, while XRD patterns indicated predominantly amorphous structures that enhance adsorption capacity. FTIR spectra confirmed the presence of hydroxyl, carbonyl and aromatic functional groups responsible for pesticide–adsorbent interactions. HPLC and GC-MS analyses verified the presence of imidacloprid and related residues prior to treatment. Batch studies showed that removal efficiency increased with higher adsorbent dose and contact time, indicating improved availability of active sites. Kinetic analysis followed pseudo-second-order behaviour, suggesting chemisorption as the rate-limiting step. Isotherm modelling using Langmuir, Freundlich and Temkin models exhibited high correlation coefficients, indicating favourable adsorption characteristics and combined surface interactions. Among the studied biomaterials, *Z. jujuba* showed the highest adsorption performance, followed by *M. indica* and *L. chinensis*. Post-adsorption GC-MS results confirmed significant reduction of pesticide-related peaks, demonstrating effective removal. These findings indicate that fruit seed-derived bioadsorbents, particularly *Z. jujuba*, are promising low-cost and sustainable materials for pesticide removal from water.

ACKNOWLEDGEMENTS

The authors express their sincere gratitude to the Department of Chemistry, Dr. C.V. Raman University, Bilaspur, India, for providing the necessary research laboratory facilities to carry out this research work.

CONFLICT OF INTEREST

The authors declare that there is no conflict of interests regarding the publication of this article.

DECLARATION OF AI-ASSISTED TECHNOLOGIES

During the preparation of this manuscript, the authors used an AI-assisted tool(s) to improve the language. The authors reviewed and edited the content and take full responsibility for the published work.

REFERENCES

1. F. Mugagga and B.B. Nabaasa, *Int. Soil Water Conserv. Res.*, **4**, 215 (2016); https://doi.org/10.1016/j.iswcr.2016.05.004
2. N. Khatri and S. Tyagi, Front. Life Science, **8**, 23 (2015); https://doi.org/10.1080/21553769.2014.933716
3. J. Qu and J. Peng, *Water Ecol.*, **1**, 100002 (2025); https://doi.org/10.1016/j.wateco.2025.100002
4. M.S. Jung, J.A.G. Da Silva, J.M. Fachinetto, I.R. Carvalho, O.A. Lucchese, N.C.F. Basso, C.M. Copetti and L.G. Da Silva, *Rev. Gest. Soc. Ambient.*, **17**, e03661 (2023); https://doi.org/10.24857/rgsa.v17n7-013
5. A. Das and S. Mishra, *GRN Tech. Res. Sustain.*, **5**, 5 (2025); https://doi.org/10.1007/s44173-025-00022-8
6. A. Müller, H. Österlund, J. Marsalek and M. Viklander, *Sci. Total Environ.*, **709**, 136125 (2020); https://doi.org/10.1016/j.scitotenv.2019.136125
7. S. Sefali, R. Ruby, D. Dimple and A. Giri, *Discov. Environ.*, **4**, 43 (2026); https://doi.org/10.1007/s44274-026-00557-y
8. M. O'Driscoll, S. Clinton, A. Jefferson, A. Manda and S. McMillan, *Water*, **2**, 605 (2010); https://doi.org/10.3390/w2030605
9. N. Khatri and S. Tyagi, *Front. Life Sci.*, **8**, 23 (2015); https://doi.org/10.1080/21553769.2014.933716
10. C. Cheng, F. Zhang, J. Shi and H.T. Kung, *Environ. Sci. Pollut. Res. Int.*, **29**, 56887 (2022); https://doi.org/10.1007/s11356-022-21348-x
11. R.K. Mishra, S.S. Mentha, Y. Misra and N. Dwivedi, *Water-Energy Nexus*, **6**, 74 (2023); https://doi.org/10.1016/j.wen.2023.08.002
12. M. Bhadarka, D. Vaghela, K. Bamaniya, H. Sikotariya, N. Kharadi, M. Bamaniya, K. Makwana and P. Verma, Water pollution: Impacts on environment (2024).
13. M.N. Issac and B. Kandasubramanian, *Environ. Sci. Pollut. Res. Int.*, **28**, 19544 (2021); https://doi.org/10.1007/s11356-021-13184-2
14. G.R. Varatharajan, J.C. Ndayishimiye and P. Nyirabuhoro, *Water*, **17**, 2367 (2025); https://doi.org/10.3390/w17162367
15. A. Zaghloul, M. Saber, S. Gadow and F. Awad, *Bull. Natl. Res. Cent.*, **44**, 127 (2020); https://doi.org/10.1186/s42269-020-00385-x
16. H.A. Areti, A.S. Hamda, L.D. Abo, A. Jabesa and M.D. Muleta, *Environ. Adv.*, **19**, 100610 (2025); https://doi.org/10.1016/j.envadv.2025.100610
17. K. Mohanrasu, A.C.M. Manivannan, H.J.R. Rengarajan, R. Kandaiah, A. Ravindran, L. Panneerselvan, T. Palanisami and C.I. Sathish, *NPJ Mater. Sustain.*, **3**, 13 (2025); https://doi.org/10.1038/s44296-025-00057-9
18. S. Meftah, K. Meftah, N. Babassa, K. Malous, M. Drissi, A. Amahrous, N. Jabri, J. Fathi, K. Aguerchi, Y. Laababid, O. Adnouss, M. Taib, O. Zinaoui, O. ElHassan and L. Bouyazza, *Discov. Sustain.*, **6**, 971 (2025); https://doi.org/10.1007/s43621-025-01359-7
19. A. Rahmani, Z. Torkshavand, K. Yari, A. Shabanloo, M. Foroghi, B. Gholazrkhogaste and R. Najafi-Vosough, *Curr. Res. Green Sustain. Chem.*, **9**, 100426 (2024); https://doi.org/10.1016/j.crgsc.2024.100426
20. E. Shumiye, T.T. Nadew, T.S. Tedla, B. Getiye, D.A. Mengie and A.G. Ayalew, *J. Water Sanit. Hyg. Dev.*, **14**, 122 (2024); https://doi.org/10.2166/washdev.2024.278
21. L.F. Cusioli, D. Mantovani, R. Bergamasco, A.M. Tusset and G.G. Lenzi, *Processes*, **11**, 2478 (2023); https://doi.org/10.3390/pr11082478
22. M.R.R. Kooh, M.K. Dahri, L. Lim and L.-H. Lim, *Arab. J. Sci. Eng.*, **41**, 2453 (2016); https://doi.org/10.1007/s13369-015-1877-5
23. S. Bhowmik, V. Chakraborty and P. Das, *Surf. Interfaces*, **3**, 100011 (2021); https://doi.org/10.1016/j.rsurfi.2021.100011
24. R. Vaiškūnaitė, *Processes*, **12**, 2560 (2024); https://doi.org/10.3390/pr12112560
25. S.S. Gabr, M.F. Mubarak, M. Keshawy, I.E.T. El Sayed and T. Abdel Moghny, *Appl. Water Sci.*, **13**, 230 (2023); https://doi.org/10.1007/s13201-023-02018-w
26. R. Ezzati, *Chem. Eng. J.*, **392**, 123705 (2020); https://doi.org/10.1016/j.cej.2019.123705
27. M. Musah, Y. Azeh, J. Mathew, M. Umar, Z. Abdulhamid and A. Muhammad, *J. Sci. Technol.*, **4**, 20 (2022); https://doi.org/10.4314/cajost.v4i1.3
28. A.O. Dada, F.A. Adekola, E.O. Odebunmi, A.S. Ogunlaja and O.S. Bello, *Sci. Rep.*, **11**, 16454 (2021); https://doi.org/10.1038/s41598-021-95090-8
29. B. Brazesh, S.M. Mousavi, M. Zarei, M. Ghaedi, S. Bahrani and S.A. Hashemi, *Interface Sci. Technol.*, **33**, 587 (2021); https://doi.org/10.1016/B978-0-12-818805-7.00003-5
30. S. Iftekhar, V. Srivastava and M. Sillanpää, *Adv. Water Treatment*, **505**, 505 (2020); https://doi.org/10.1016/B978-0-12-819216-0.00007-2
31. M. Murugesan and M. Pulimi, *Chem. Africa*, **8**, 2439 (2025); https://doi.org/10.1007/s42250-025-01372-3
32. U.A. Qureshi, B.H. Hameed and M.J. Ahmed, *J. Water Process Eng.*, **38**, 101380 (2020); https://doi.org/10.1016/j.jwpe.2020.101380

33. S. Cui, J. Lv, R. Hough, Q. Fu, Z. Zhang, X. Dong, X. Fan and Y.-F. Li, *Environ. Res.*, **258**, 119444 (2024); https://doi.org/10.1016/j.envres.2024.119444
34. Y. Ma, Y. Qi, T. Lu, L. Yang, L. Wu, S. Cui, Y. Ding and Z. Zhang, *Sci. Total Environ.*, **765**, 144253 (2021); https://doi.org/10.1016/j.scitotenv.2020.144253
35. X. Ji, Y. Liu, Z. Gao, H. Lin, X. Xu, Y. Zhang, K. Zhu, Y. Zhang, H. Sun and J. Duan, *Sep. Purif. Technol.*, **330**, 125235 (2024); https://doi.org/10.1016/j.seppur.2023.125235
36. Y. Chen, M. Hassan, M. Nuruzzaman, H. Zhang, R. Naidu, Y. Liu and L. Wang, *Environ. Sci. Pollut. Res. Int.*, **30**, 4754 (2023); https://doi.org/10.1007/s11356-022-22357-6
37. Y. Ma, S. Chen, Y. Qi, L. Yang, L. Wu, L. He, P. Li, X. Qi, F. Gao, Y. Ding and Z. Zhang, *Chemosphere*, **291**, 132707 (2022); https://doi.org/10.1016/j.chemosphere.2021.132707